# Effects of degree of compaction and fines content of the subgrade bottom layer on moisture migration in the substructure of high-speed railways

**Ren-Peng Chen[1,2], Han-Lin Wang[1], Peng-Yun Hong[2], Yu-Jun Cui[3], Shuai Qi[1] and Wei Cheng[1]**

## Abstract

Moisture migration and distribution in the substructure are found to be the important reasons for water-related problems in high-speed railways. In this study, a numerical model of a double-line ballastless track-bed consisting of a substructure (subgrade surface layer, subgrade bottom layer and subsoil) and a superstructure (including two concrete bases right above the substructure) was established. The superstructure was considered as an impermeable boundary in this model, while two fissures were set at the joint edges of the left-line concrete base and the surface layer, simulating the infiltration area of rainwater. The effects of degree of compaction and fines content of the bottom layer due to moisture migration in the high-speed railway substructure were investigated on this model by applying and analyzing the 2013 rainfall data of Hangzhou, China, for a three-year period. The results show that the saturation zones develop in the subgrade, after a three-year period, with the size increasing with the increase in the degree of compaction or fines content due to higher water retention capacity and lower permeability of the soil. Furthermore, the variations of volumetric water content at different depths of the left-fissure profile indicate that as the degree of compaction or fines content increases, the arriving time of the wetting front increases, but the fluctuation amplitude of the volumetric water content after the arrival of the wetting front decreases on the whole. The degree of compaction appears to present a more significant impact on these two parameters. In particular, a threshold value of the degree of compaction between 0.90 and 0.93 is observed, prolonging the arriving time of the wetting front remarkably at a certain elevation. Besides, it takes a longer time for the wetting front to pass through the interface between the surface layer and the bottom layer for each case. From a practical point of view, it will be beneficial to employ drainage methods to drain out the water before it reaches the bottom layer.

## Introduction

Due to its lower life-cycle cost compared to the conventional railway lines, ballastless track-bed has been widely used in newly constructed high-speed railways in China; till 2015, the total running mileage of high-speed railways has reached 16,000 km, of which 70% are ballastless. In general, the ballastless track-bed mainly consists of two parts: superstructure and substructure. The superstructure includes rail, fastener, track slab, cement asphalt layer, and concrete base. The substructure is composed of subgrade surface layer (SSL), subgrade bottom layer (SBL), and subsoil. As the intermediate structure between the superstructure and the subsoil, the subgrade plays a key role in maintaining the long-term serviceability of high-speed railways. According to TB10621-2009, the designing life of the subgrade is

[1]MOE Key Laboratory of Soft Soils and Geoenvironmental Engineering, Department of Civil Engineering, Zhejiang University, Hangzhou, China
[2]School of Civil Engineering, Hunan University, Changsha, China
[3]Laboratoire Navier/CERMES, Ecole des Ponts ParisTech, Champs-sur-Marne, France

**Corresponding author:**
Ren-Peng Chen, Zhejiang University, 866 Yuhangtang Road, Hangzhou, China.
Email: chenrp@zju.edu.cn

100 years.[1] Moreover, previous studies indicate that the water-related problems in the subgrade is one of the main challenges in the maintenance of existing high-speed railways.[2–8] Therefore, understanding the moisture migration patterns in the substructure is of paramount importance for ensuring the track-bed operating performance during its service life.

Under long-term cyclic loading, fissures develop mainly in two areas in the track-bed[8]: (1) the interspace area filled with asphalt between the two neighboring concrete bases in the moving direction of a train; (2) the joint edge between the concrete base and SSL, the area in which the stress concentration is observed.[9] In rainy days, ponding develops in the fissures and then rainwater migrates into the SSL through the fissures. Without efficient drainage facilities, water cannot be easily drained out. As a result, with the increase of water content, parts of the unsaturated geomaterials turn into saturated ones. Thus, the matric suction decreases and the mechanical performance of the subgrade deteriorates accordingly. Then, under cyclic loading, it may lead to water-related problems characterized as mud pumping, differential settlement, etc.

It has been proven that water-related problems are closely linked to moisture distribution and migration in the substructure.[5,8,10] The phenomenon of moisture migration has been studied extensively in unsaturated fine-grained soils such as silty soils and loess by experimental methods. It was found that the moisture migration in these soils was mainly dependent on compaction state, initial water content, and temperature gradient.[11–14] In addition, some analytical–numerical models of infiltration were proposed to predict moisture migration in unsaturated slopes, highway pavement, etc.[15–17] However, for the coarse-grained materials of SSL and SBL in high-speed railways, the hydraulic properties are distinctively different from those of fine-grained soils. Hence, moisture migration and distribution in these materials are expected to exhibit quite different patterns. To date, research studies on moisture migration in coarse-grained soils are still scarce. It remains

unknown whether the existing experimental results or empirical formulae from fine-grained soils can be directly applied to estimate moisture migration in the high-speed railway substructure. Additionally, infiltration through fissures developed in high-speed railway track-bed has been rarely investigated.

In this study, a numerical model was established to simulate the moisture migration in the high-speed railway substructure due to rainfall. Five cases of SBL with different degrees of compaction and fines contents were considered. Two fissures were set at the joint edges of the left-line concrete base and SSL to simulate the infiltration area. The 2013 rainfall data of Hangzhou, China were applied and repeated for three-year calculation. The numerical results show the effects of degree of compaction and fines content of SBL on the moisture migration and distribution in the substructure.

## Numerical modeling

### Overview of the model and boundary conditions

A numerical model of a double-line high-speed railway track-bed containing superstructure (including two concrete bases in this study) and substructure is established in accordance with TB10621-2009.[1] Figure 1 shows the schematic view of this model. It can be observed that the substructure consists of three layers including SSL, SBL, and subsoil.

For the boundary conditions, the concrete bases (lines 6 and 9) are set as impermeable boundaries (shown by solid lines in Figure 1). The upper surface of SSL is covered by thin concrete slabs according to TB10621-2009.[1] Thus, the relevant boundaries (lines 4, 8, and 10) are also set to be impermeable. The slopes of the substructure should be protected by some measures such as growing plants or draining channels after construction according to TB10621-2009.[1] Rainwater is hard to infiltrate through the slopes in rainy days, so infiltration through the slopes is not considered in this model. However,
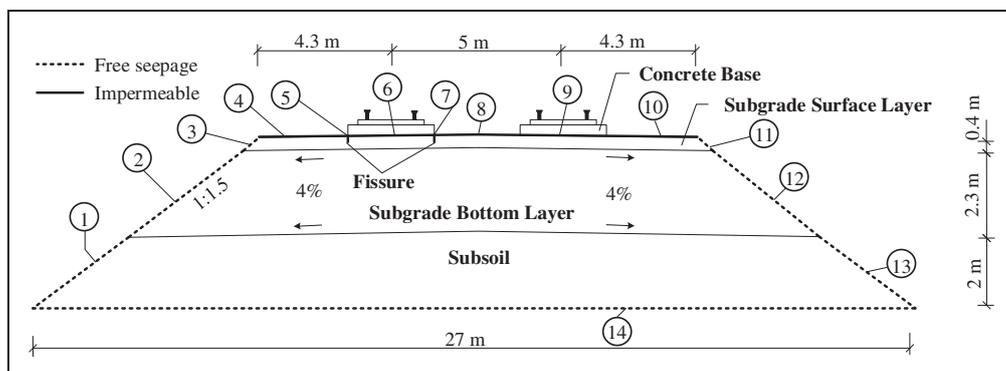


**Figure 1.** Numerical model of ballastless high-speed railway track-bed. Numbers in circles represent the boundaries of the model. Different line types represent different boundary conditions.

when infiltrated water migrates near the slopes of substructure, it can be drained out due to water accumulation. Thus, the slopes (lines 1, 2, 3, 11, 12 and 13) are considered as the free seepage boundaries (shown by dotted lines in Figure 1), and infiltration of rainwater from the slopes is not taken into account. The bottom boundary of this model (line 14) is set as the free seepage boundary.

Two fissures of 0.01 m width and 0.1 m length are located at the joint edges of the left-line concrete base and SSL (Figure 1) to simulate infiltration boundaries which have been identified in the field.[8] The boundary conditions (lines 5 and 7) are categorized into two cases. When the daily precipitation is no more than 5 mm, it is assumed that no ponding develops at the surface of the fissures. The boundaries are considered to be impermeable. Otherwise, ponding is assumed to develop when the daily precipitation exceeds 5 mm. In this case, the boundaries are set to be submitted to zero water pressures by considering that the ponding head is not high. The duration time of the zero pressure boundaries will be illustrated in the following section.

Five cases of SBL materials with different degrees of compaction and fines contents are considered. The specific properties of the five SBL materials are listed in Table 1. Simulated rainfall conditions are based on the daily precipitation data of Hangzhou, China in 2013. Three circulations representing three years were considered with these rainfall data. Moisture migration was calculated for each case using Geo-Studio Seep/W.

## Materials

Different materials are set to represent SSL, SBL, subsoil, and fissures. For seepage problems, two hydraulic properties are used: hydraulic conductivity function (HCF) and soil water retention curve (SWRC).

Graded gravel with clay and sand is selected to simulate the material of SSL.[18] This material is classified as GPGC according to ASTM D2487-11.[19] The gradation is in correspondence with TB10621-2009 (Figure 2).[1] The hydraulic properties are shown in Figures 3 and 4.

The materials of SBL are taken from a subgrade filling site in Hangzhou, China. Five different kinds of SBL materials are compared. Different degrees of compaction and fines (particle size smaller than 0.075 mm) contents are set to distinguish the five cases (Table 1). The gradations are shown in Figure 2 and they are in accordance with TB10621-2009.[1] The SWRC and saturated hydraulic conductivity of these materials were measured using a large-scale infiltration column.[20–22] For technical reason, particles larger than 20 mm were excluded from the experiment. van Genuchten's model[23] was used to fit the hydraulic properties of these five materials (Figures 3 and 4).

The hydraulic properties of the subsoil are derived from one kind of silt as shown in Figures 3 and 4.[24] This material can be classified as ML according to ASTM D2487-11[19] and it meets the requirement of TB10621-2009.[1]

Fractured rocks are selected as the material of fissures. The SWRC and HCF of fissures are investigated by Zhang and Fredlund[25] and Chae et al.,[26] respectively (Figures 3 and 4). The parameters of these two materials are similar and it is reasonable to use both materials simultaneously.

For all materials, the optimum volumetric water content is the initial condition in practical engineering.[1] With the optimum volumetric moisture content, the initial matric suction and hydraulic conductivity of all materials can be determined through SWRC and HCF. The initial parameters are listed in Table 2.

## Analyses of rainfall conditions

The data of daily precipitation of Hangzhou, China in 2013 is provided by the Weather Bureau of Hangzhou as shown in Figure 5.

As it is difficult to apply the daily precipitation data directly into the numerical model, the duration of rainfall is transited from daily precipitation using the method proposed by Wang et al.[27] An empirical formula dealing with the relationship between average
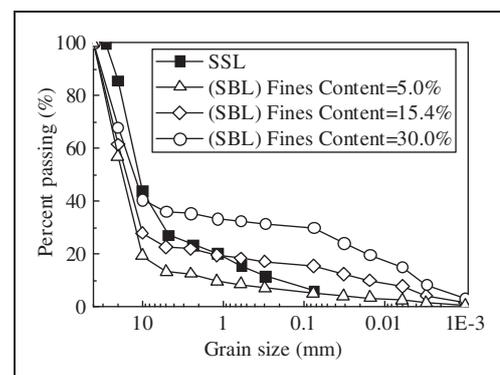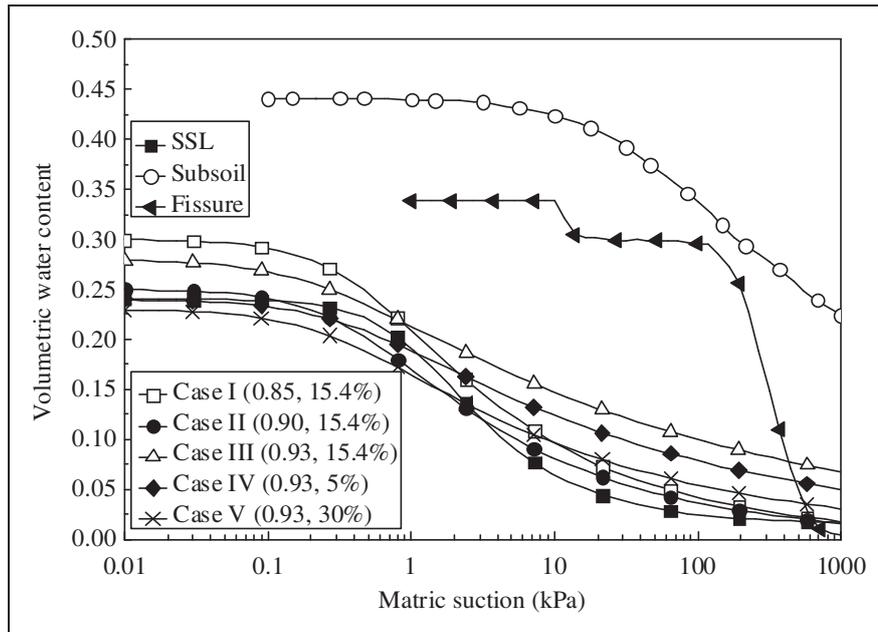


Figure 2. Gradations of SSL and SBL.

**Table 1.** Properties of five different SBL materials.[a]

| Subgrade category | Case I | Case II | Case III | Case IV | Case V |
|---|---|---|---|---|---|
| Degree of compaction | 0.85 | 0.90 | 0.93 | 0.93 | 0.93 |
| Fines content (%) | 15.4 | 15.4 | 15.4 | 5.0 | 30.0 |

[a]Case I, II, III, IV, and V represent the corresponding SBL materials and these annotations are available in the following page.

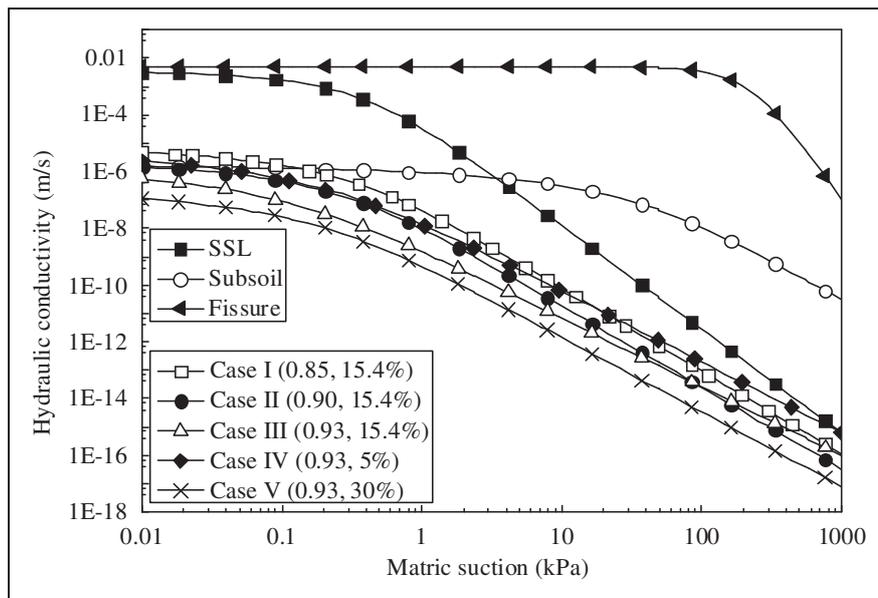**Figure 3.** SWRC of all materials.



**Figure 4.** Hydraulic conductivity of all materials.

rainfall intensity $i$ and rainfall duration time $t$ is used[28]

$$i = \frac{S}{t^n} \tag{1}$$

where $n$ is the damping coefficient which illustrates the concentration of total rainfall in time $t$; $S$ is the maximum value of rainfall intensity per unit time.

For the value of $S$, an empirical model related with the daily precipitation $I$ was proposed by Zhou et al.[29] as

$$S = a_i I + b_i \tag{2}$$

where $a_i$ and $b_i$ are the empirical coefficients.

Then, based on the assumption that the rainfall in one rainy day is continuous without time intervals, the daily precipitation $I$ can be determined as follows
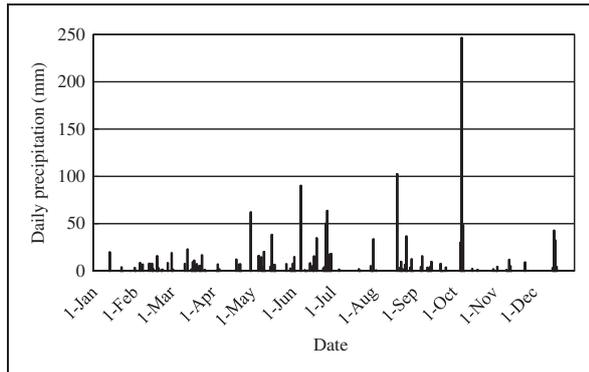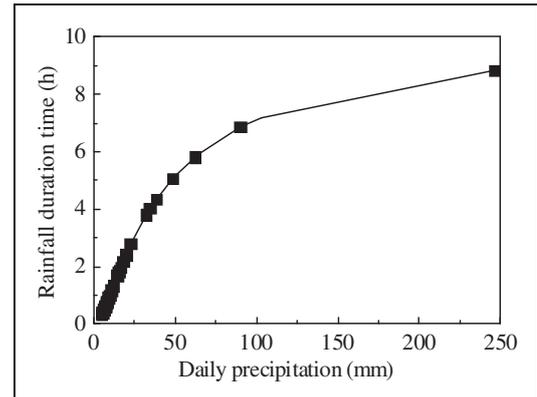
$$I = it \tag{3}$$

By combining equations (1) to (3), a relationship between rainfall duration time $t$ and daily precipitation $I$ can be determined as

$$t^{n-1} = a_i + \frac{b_i}{I} \tag{4}$$

**Table 2.** Initial parameters of all materials.

| Parameters | SSL | Subsoil | Fissure | Case I | Case II | Case III | Case IV | Case V |
|---|---|---|---|---|---|---|---|---|
| $w_{opt}$ (%) | – | – | – | 5.9 | 5.9 | 5.9 | 4.0 | 7.0 |
| $\rho_{dmax}$ (g/cm$^3$) | – | – | – | 2.33 | 2.33 | 2.33 | 2.41 | 2.17 |
| $\theta$ (%) | 10.0 | 29.5 | 10.0 | 13.7 | 13.7 | 13.7 | 9.6 | 15.2 |
| $\Psi$ (kPa) | 13.2 | 185.8 | 389.1 | 3.8 | 2.1 | 15.4 | 34.8 | 1.5 |
| $K$ (m/s) | 4.56e−9 | 2.54e−9 | 4.61e−5 | 1.24e−9 | 1.44e−9 | 2.38e−12 | 2.73e−12 | 1.88e−10 |

$w_{opt}$: optimum gravimetric water content; $\rho_{dmax}$: maximum dry density; $\theta$: volumetric moisture content; $\Psi$: matric suction; $K$: hydraulic conductivity.



**Figure 5.** Daily precipitation of Hangzhou, China in 2013.



**Figure 6.** Relationship between rainfall duration time and daily precipitation.

Using the empirical parameters $a_i = 0.3622$, $b_i = 6.376$, and $n = 0.565$ proposed by Zhou et al.,[29] a fitting relationship between rainfall duration time and daily precipitation is obtained as shown in Figure 6. Using this fitting relationship and the measured daily precipitation data (Figure 5), the rainfall duration time of zero pore pressure boundary for the fissures can be determined and applied to the numerical model.

## Numerical results

### Development of saturation zone

When infiltrating into the subgrade through fissures, rainwater migrates both laterally and vertically due to the heterogeneous pore channels of coarse-grained soils. As the infiltration areas are in the center of the subgrade, water cannot be drained out immediately. When more water gets accumulated, some unsaturated regions of the subgrade become saturated, i.e. a saturation zone develops. Over time, water in these areas can still migrate down to form new saturation zones or the original small ones can expand. After a long period some water can be drained out from the subgrade or migrate down to deeper layers, while the remaining will accumulate to form larger saturation zones.

In order to investigate the development of saturation zones, Figure 7 compares the results of the five simulated cases after one-year, two-year, and three-year period. The saturation zones in this figure are

plotted by bold lines. Note that the bottom lines of the saturation zones after a specific period are the same for all cases, so they are set as the same solid lines without symbols. From this figure, it can be observed that saturation zones develop in the subgrade and water accumulates at the interface of SBL and subsoil. This is due to the extremely low hydraulic conductivity of the subsoil at unsaturated state. For instance, the initial matric suction of subsoil (185.84 kPa) corresponds to the unsaturated hydraulic conductivity of $2.54 \times 10^{-9}$ m/s (see Figure 4). It is much lower than the saturated value of SBL and thus moisture migration from the subgrade to the subsoil proceeds slowly. Besides, the saturated volumetric water content of subsoil is as high as 0.45 and the bottom boundary of subsoil is seepage free. Hence, the small amount of water infiltrating into the subsoil is not sufficient to saturate this layer and the infiltrated water can continue to migrate downwards until outside this model. Note also that because of the free seepage boundaries set at the bottom and the slopes of the model, the water cannot accumulate at the bottom of this model and the water table cannot be elevated either during the rainfall.

For the SBL with fines content of 15.4%, the size of saturation zone after the three-year calculation period expands with the increase of degree of compaction (Figure 7). This observation can be explained as follows. For the saturation zone, the soil starts to turn into unsaturated state in dry days as suction increases
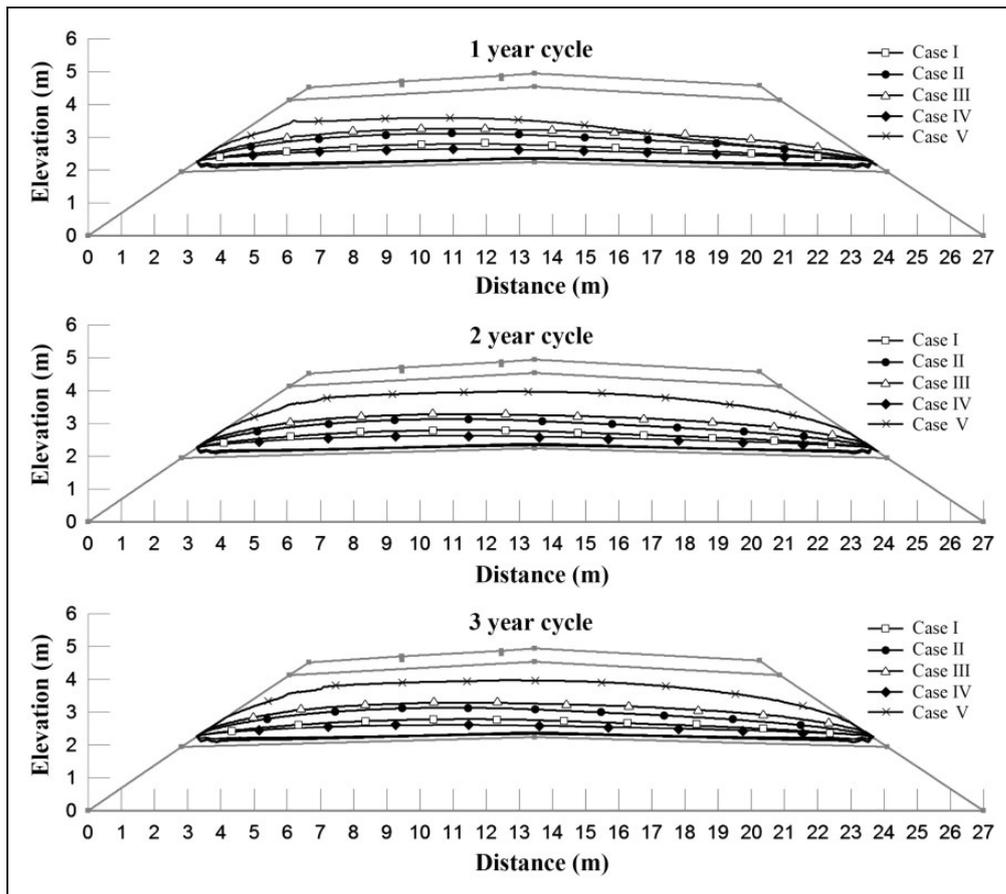
**Figure 7.** Development of saturation zone after one-year, two-year, and three-year period.

beyond the air entry value. In this case, the water retention capacity is mainly controlled by the capillary effect, which is highly influenced by the particle and pore size: the soils with smaller particle and pore sizes present higher capillary effect.[30,31] In the coarse-fine mixed soil such as the SBL, macropores formed by the voids of coarse grains and micropores between fine particles exist.[32] As the degree of compaction increases the micropores stay unchanged whereas the macropores become smaller.[33] With smaller macropores, the capillary effect tends to increase, leading to higher water retention capacity. However, compared to the capillary effect developed by the micropores, the influence of macropores appears to be less pronounced.[31] Therefore, with unchanged micropores and smaller macropores, the capillary effect increases slightly with the increase of degree of compaction. As a result, the water retention capacity or the size of saturation zone increases as the degree of compaction increases, but the influence is not significant.

For the SBL with compaction degree of 0.93, it has been indicated in Figure 7 that after the three-year calculation period, the size of the saturation zone of case V (0.93, 30%) is about two times larger than that of case III (0.93, 15.4%) and three times larger than case IV (0.93, 5%). Note that with fines content

increasing, the water retention capacity increases accordingly. In addition, the hydraulic conductivity curve of case V (0.93, 30%) lies beneath those of case III (0.93, 15.4%) and case IV (0.93, 5%) (Figure 4). Case V (0.93, 30%) has a lower permeability and it is difficult for water to be wiped out comparatively.

To make a better analysis about the influences of degree of compaction and fines content on the development of saturation zone, a parameter $\delta$ is introduced, defined as the area ratio of saturation zone to the whole substructure (subgrade and subsoil), after the three-year period. Figure 8 shows the variation of $\delta$ versus these two impact factors. The fitting relationships between $\delta$ and the two parameters are also plotted in Figure 8. Both fitting relationships are linear. The values of 0.85 and 0.93, respectively, represent low and high degrees of compaction in practice. For the fines content of 15.4%, with the degree of compaction degree rising from 0.85 to 0.93, $\delta$ increases by 98.8% (Figure 8(a)), whereas for the degree of compaction 0.93, with fines content ranging from 5% to 30%, $\delta$ increases by 276.1% (Figure 8(b)). This rate of increment is much larger than that influenced by the degrees of compaction. In other words, the size of saturation zone is more influenced by fines content than by the degree of compaction.
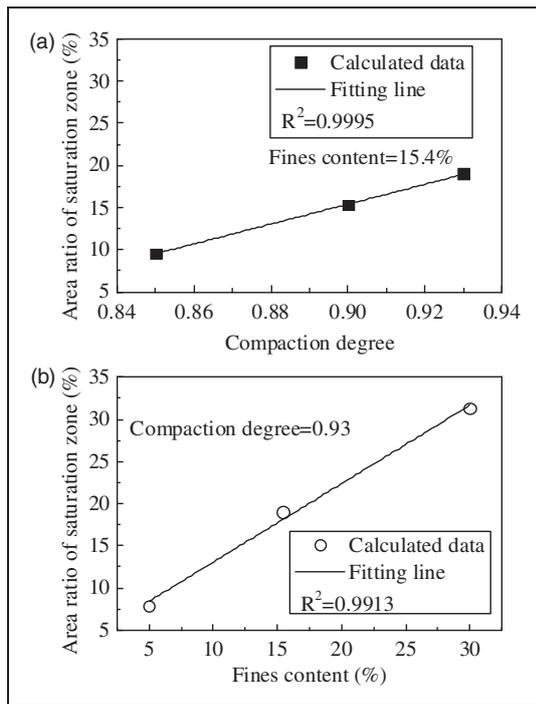
**Figure 8.** Relationship between $\delta$ and (a) degree of compaction (fines content $=$ 15.4%); (b) fines content (degree of compaction $=$ 0.93).

### Variation in volumetric water content

The variations in volumetric water content ($\theta$) are further analyzed based on the left-fissure profile at five different levels (Figure 9). This profile is selected because it can be the most dangerous area, i.e. an area with direct infiltration. Point A ($h = 4.6$ m) represents the center area in the SSL. Point B ($h = 4.2$ m) represents the top area of SBL, 0.2 m below the interface of SSL and SBL. Point C ($h = 3.5$ m) and point D ($h = 2.9$ m) represent the center area in the SBL. Point E ($h = 2.3$ m) represents the bottom area of SBL, 0.2 m above the interface of SBL and subsoil. Note that the points on the interface are not chosen since the factors influencing moisture migration at the interface are more complicated and it is difficult to differentiate all the impact parameters. Therefore, two points close to the interfaces (point B and point E) are selected instead of them.

Figure 10 shows the typical variation trend of volumetric water content with time (at point B, case III). It can be observed that before about 72 days, the $\theta$ value stays stable at the initial volumetric water content. After 72 days, $\theta$ increases significantly to higher values, suggesting that a saturated "interface" reaches and passes this area. This "interface" is defined as the wetting front (Figure 10), separating the infiltrated soil (nearly saturated) and the dry soil.[34,35] The time when the volumetric water content starting to rise rapidly is defined as the arriving time of the wetting front $t_{wf}$ (Figure 10). After the wetting front's arrival,

due to the rainfall, the $\theta$ value fluctuates between the minimum value $\theta_{min}$ and the maximum value $\theta_{max}$, as shown in Figure 10. In addition, for the fluctuation amplitude $\Delta\theta$, it is is defined as

$$\Delta\theta = \theta_{max} - \theta_{min} \tag{5}$$

Figures 11 to 15 plot the volumetric water content variations of the five mentioned points at the left-fissure profile. It is indicated in Figure 11 that the difference of volumetric water content variations of point A is not significant for each case, i.e. the moisture migration at this point is independent on SBL materials. Since point A lies 0.1 m right below the lower part of the fissure, the volumetric water content is influenced significantly by the climatic condition. Also, SSL has a high saturated hydraulic conductivity up to $3.2 \times 10^{-3}$ m/s. $\theta$ increases rapidly in rainy days and it drops down sharply in sunny days as water migrates downwards fast. This also leads to a wide range of $\theta$ fluctuation – from 0.10 to 0.28 at this point.

The variation in volumetric water content at point B ($h = 4.2$ m) is plotted in Figure 12. During the initial time, the volumetric water content stays stable except for case II (0.90, 15.4%) and case IV (0.93, 5%) with slight changes. Then, a sudden rise of $\theta$ takes place after the wetting front reaches this area. The arriving time of the wetting front is different for each case, due to different initial hydraulic conductivities (see Table 2). As the initial hydraulic conductivity decreases, the arriving time of the wetting front delays accordingly. After the arrival of the wetting front, a fluctuation of volumetric water content follows for all cases as illustrated in Figure 10, while the fluctuation amplitudes are different. Note that without the formation of a long-term saturation zone at this point, the volumetric water content fluctuations are similar in each year for all cases.

For point C (Figure 13), the volumetric water content variations exhibit the same evolution trend as illustrated in Figure 10, except for case V (0.93, 30%). Unlike the typical variation trend in Figure 10, after 450 days, the volumetric water content of case V (0.93, 30%) stays at the saturated value and remains unchanged till the end of calculation period. This suggests the formation of a long-term saturation zone at this high elevation, which is unfavorable to prevent water-related problems. With regard to point D (Figure 14), long-term saturation zones are also observed, in more cases except for case I (0.85, 15.4%) and case IV (0.93, 5%).

At point E near the bottom area of SBL (Figure 15), when the wetting front reaches this area, a sudden rise of volumetric water content occurs and $\theta$ remains at saturated state for all cases afterwards. Water accumulates at the interface of SBL and subsoil due to the significant difference of hydraulic conductivities between these two materials, which is verified
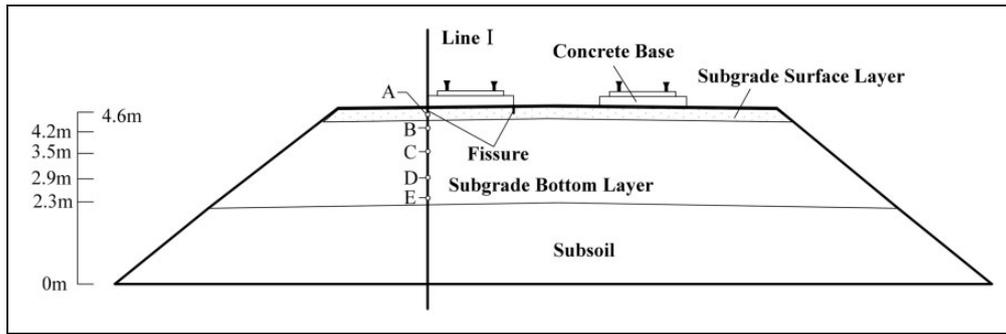
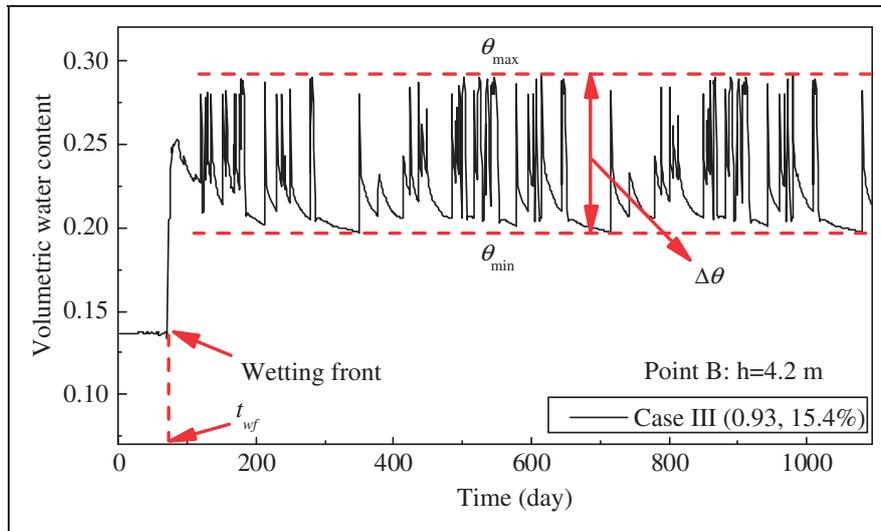**Figure 9.** Analyzed points at the left-fissure profile.



**Figure 10.** Typical variations of volumetric water content with time (at point B, case III).

in Figure 7. Only by natural seepage, the accumulated water cannot be wiped out easily. Note that the long-term saturation zones are also found in the in-situ investigations by Smethurst et al.[36] However, due to the more complex conditions in the field, the volumetric water content in these saturated areas may vary in a narrow range around the saturated state rather than staying strictly unchanged, as shown in Figures 13 to 15.

## Discussions

To illustrate the variations of volumetric water content in the subgrade, the arriving time of the wetting front $t_{wf}$ and the fluctuation amplitude of volumetric water content $\Delta\theta$ after the arrival of the wetting front are the two important parameters considered. They are observed to be influenced by both the degree of compaction and the fines content as shown in Figures 11 to 15. To have a better understanding of this phenomenon, elevations at the left-fissure profile are plotted versus $t_{wf}$ and $\Delta\theta$ in Figure 16 and Figure 17, respectively.

For the SBL with fines content of 15.4% (Figure 16(a)), the results at 0.85 and 0.90 degrees of compaction share a similar trend of $t_{wf}$ along the elevations. It takes a long time for the wetting front to migrate from 4.6 m to 4.2 m, while the time taken for the wetting front to continue migrating downwards till the bottom of SBL is much shorter. The $t_{wf}$ values for 0.90 degree of compaction under 4.2 m are higher than those for 0.85 degree of compaction, but the difference is less. In comparison, in the case of 0.93 degree of compaction, the $t_{wf}$ values show a sharp increase as the wetting front migrates from 4.6 m to 3.5 m and then the rate of increase becomes less pronounced. The values of 0.93 degree of compaction at the elevations below 4.2 m are clearly higher than the other two cases. It appears that a threshold value may exist between 0.90 and 0.93 degrees of compaction, prolonging the arriving time of the wetting front significantly. More studies are needed to clarify this issue. For the SBL with compaction degree of 0.93 (Figure 16(b)), at 5% and 15.4% fines contents, the curves almost have the same shape over 2.9 m while
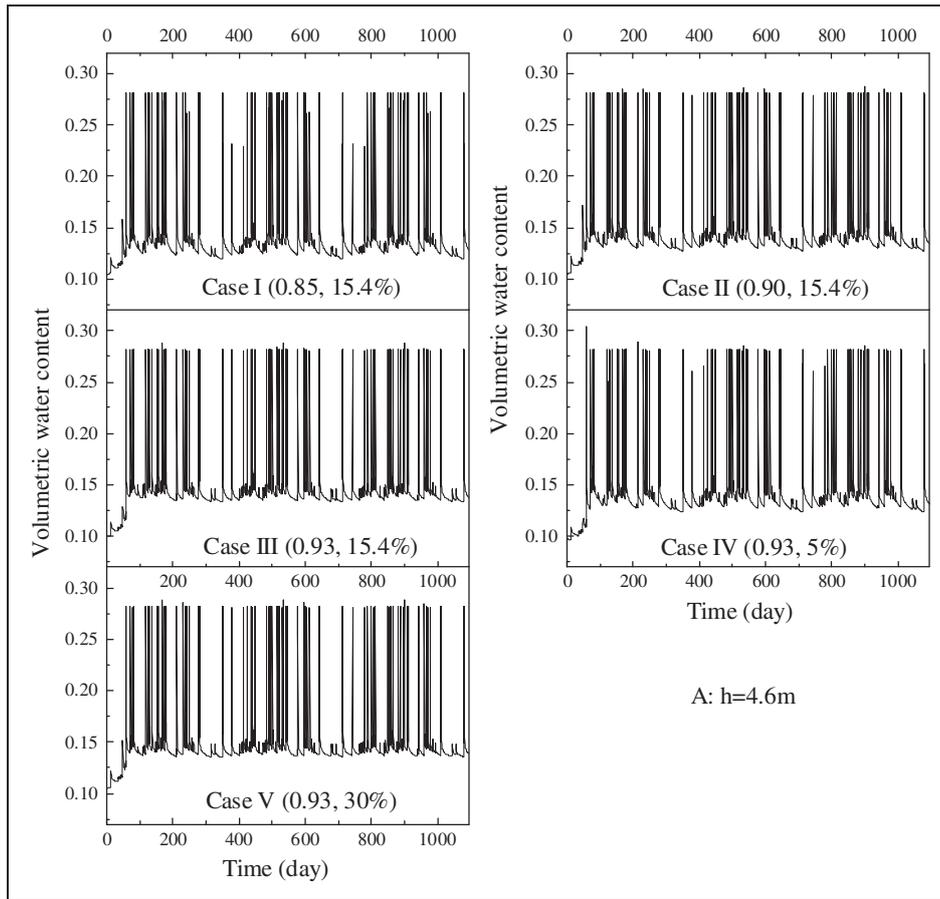
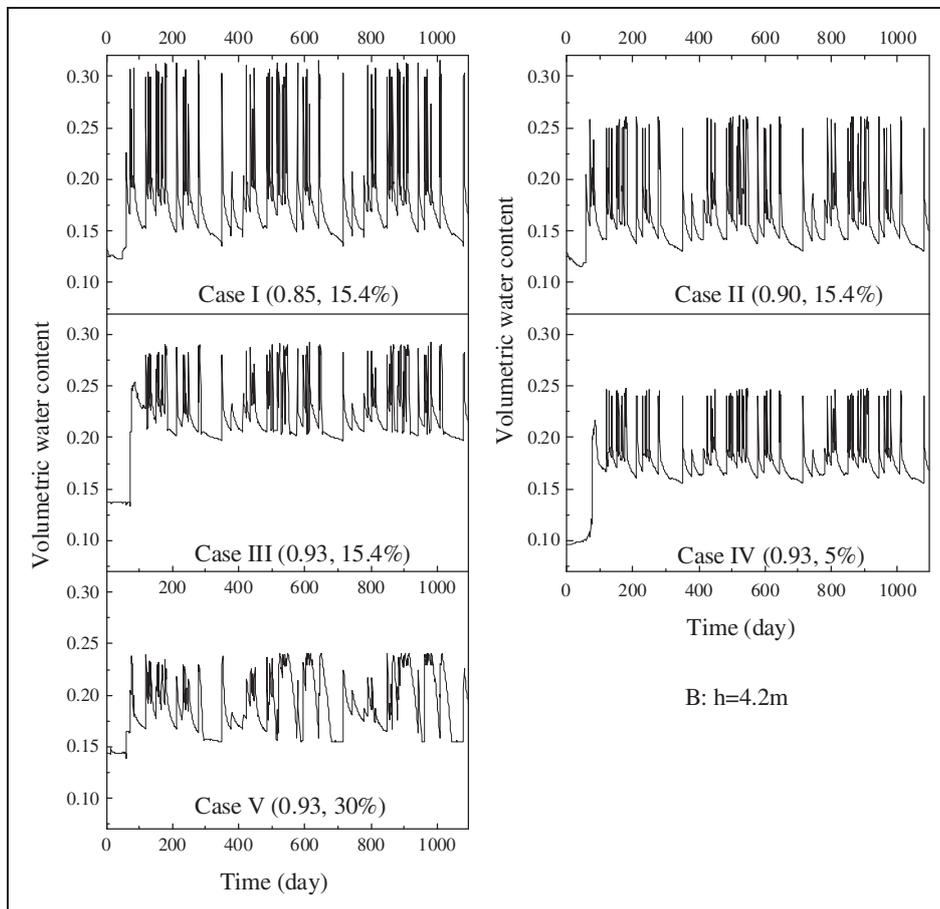**Figure 11.** Volumetric water content variations: point A.



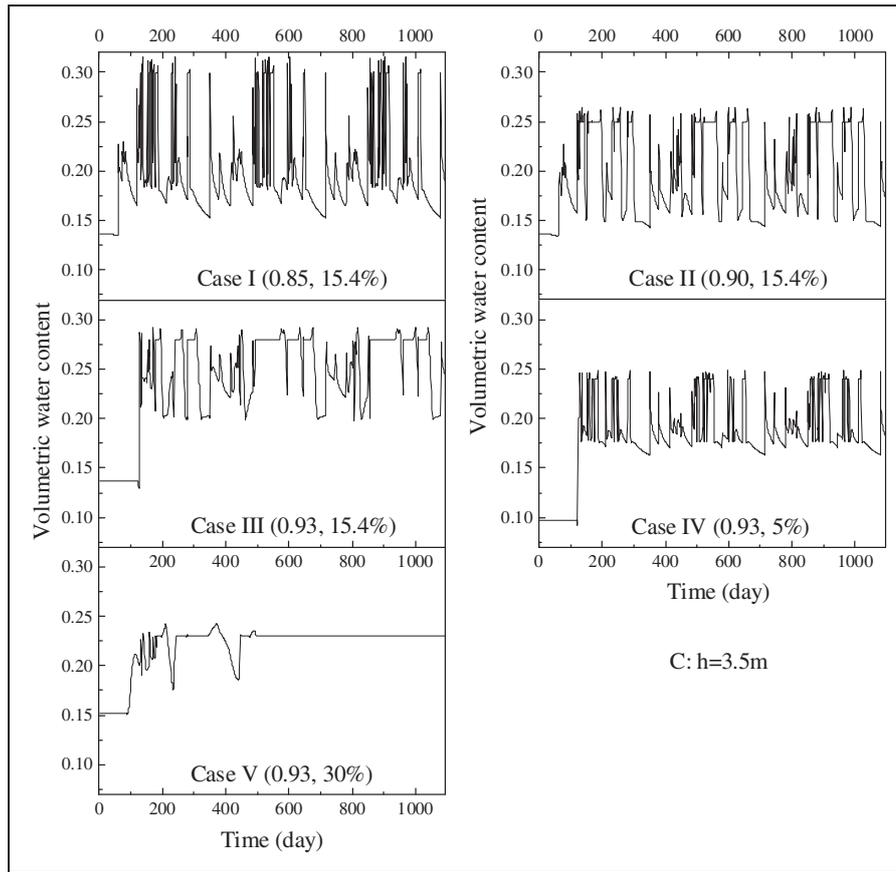**Figure 12.** Volumetric water content variations: point B.

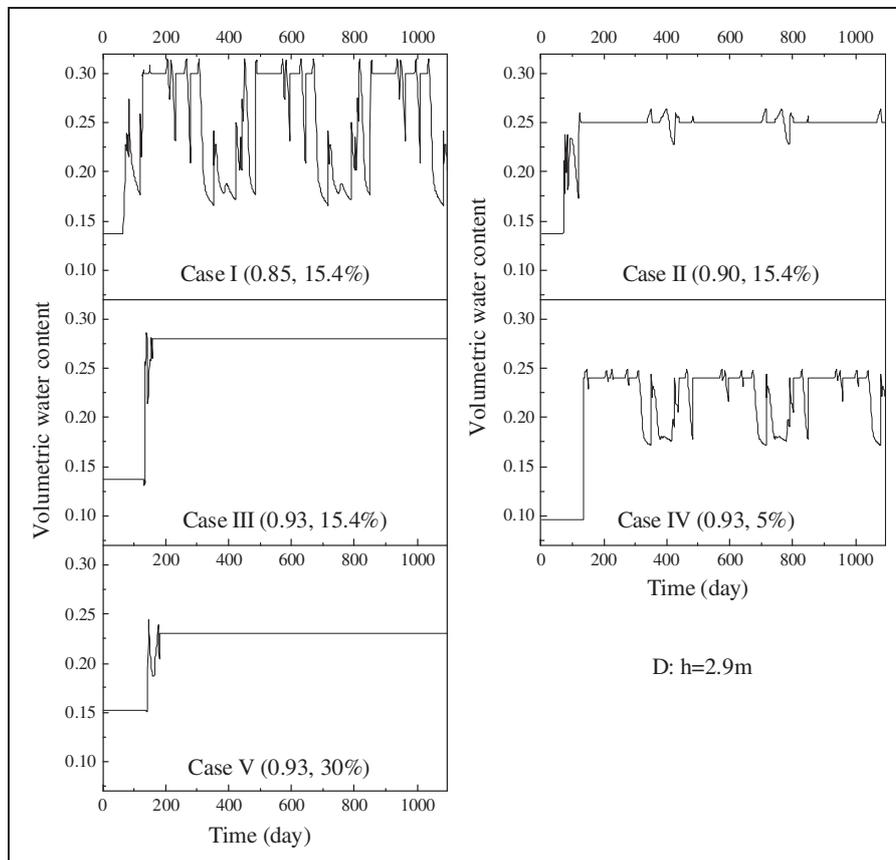**Figure 13.** Volumetric water content variations: point C.



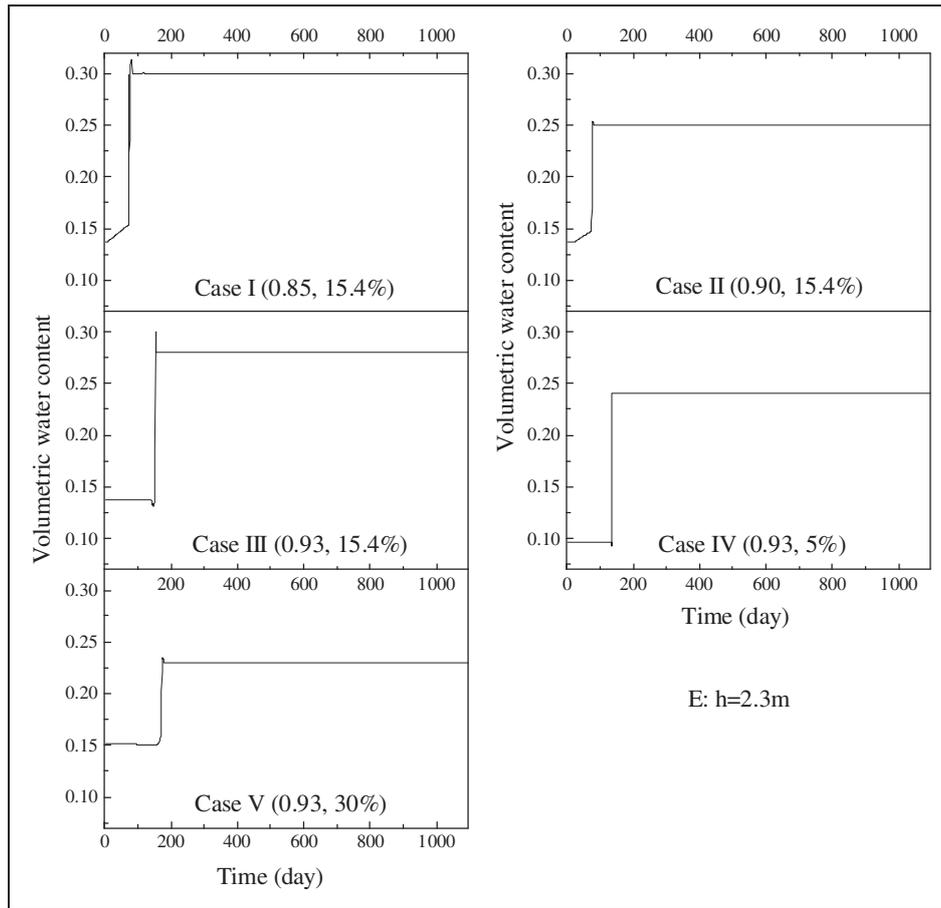**Figure 14.** Volumetric water content variations: point D.

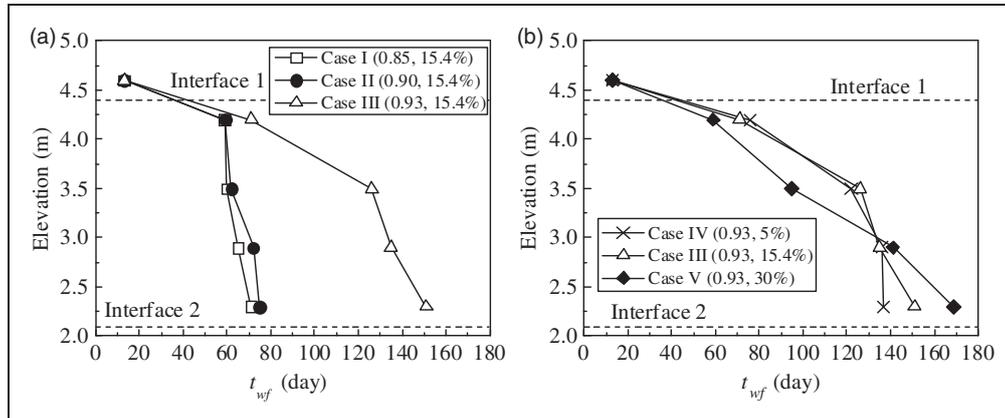**Figure 15.** Volumetric water content variations: point E.



**Figure 16.** Effects of (a) degree of compaction and (b) fines content on the arriving time of wetting front at different elevations. Note: interface 1 is the interface between SSL and SBL; interface 2 is the interface between SBL and subsoil.

the value of 15.4% at the bottom of SBL is higher than that of 5%. By contrast, at 30% fines content, the $t_{wf}$ values over 2.9 m are lower than the other two cases due to its higher initial hydraulic conductivity (see Table 2). On the contrary, the $t_{wf}$ values for 30% fines content from 2.9 m to 2.3 m are higher than the other two cases and the differences become larger in deeper elevations. This could be ascribed to a higher water retention capacity of 30% fines content. Water

can be more easily held at upper elevations and more water from infiltration is needed to move on the migration process. This also implies that the wetting front takes longer time to migrate through the whole SBL for 30% fines content.

Except for the above-mentioned analysis, it is also indicated in Figure 16 that for all cases, it takes a relatively longer time for the wetting front to pass through interface 1 (the interface between SSL and
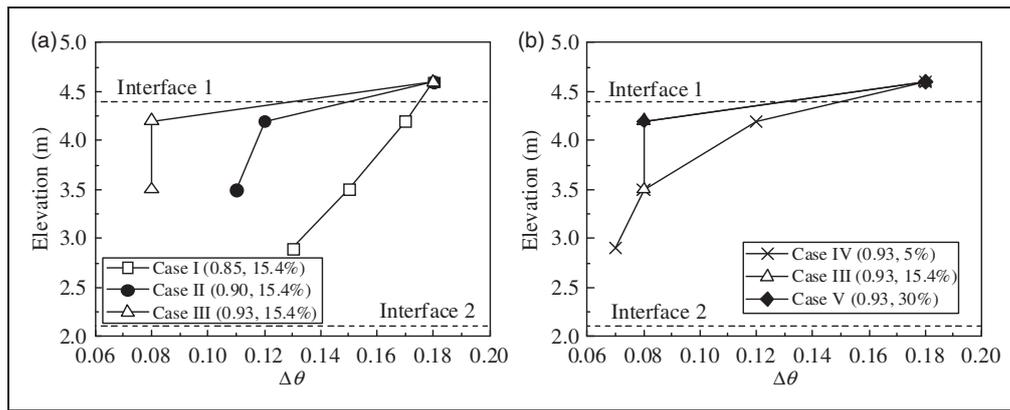
**Figure 17.** Effects of (a) degree of compaction and (b) fines content on the fluctuation amplitude of volumetric water content at different elevations. Note: interface 1: the interface between SSL and SBL; interface 2: the interface between SBL and subsoil.

SBL). This can be explained by the difference in hydraulic conductivities between SSL and SBL as shown in Figure 4. At the beginning, when rainwater migrates to the interface of SSL and SBL, little water migrates down to the SBL, while the majority stays above this interface and small saturation zones develop. It is in accordance with the designing protocol of TB10621-2009: rainwater should be drained out in the SSL before migrating down into the SBL.[1] However, without well-operated drainage systems, more water accumulates at the interface and the water content of the SBL area close to interlayer 1 becomes higher as time passes. Thus, the hydraulic conductivity in this area increases accordingly and more water migrates downwards to the SBL. Then, it leads to a sudden rise of volumetric water content at point B as shown in Figure 12. From a practical point of view, this observation is important for the subgrade maintenance. If the accumulated water above interface 1 can be drained out on time, then the problems due to saturation zone can be solved. This can be done by setting up a drainage layer between SSL and SBL. More studies are needed to verify this method.

For fluctuation amplitudes of volumetric water content $\Delta\theta$ at the selected profile, Figure 17 is plotted to illustrate the effects of degree of compaction and fines content except for the points with long-term saturation zones. For the SBL with fines content of 15.4% (Figure 17(a)), the $\Delta\theta$ value at 0.85 degree of compaction decreases linearly from 4.6 m to 2.9 m and the values are the highest compared to the other two cases, while the $\Delta\theta$ value at 0.90 and 0.93 degree of compaction decreases sharply from 4.6 m to 4.2 m and then decreases more slightly or stay stable from 4.2 m to 3.5 m. The values of 0.90 are higher than those of 0.93 at a given elevation under 4.6 m. For the three cases, the difference of $\Delta\theta$ values can be explained by the hydraulic conductivities of the materials (see Figure 4). With relatively lower hydraulic conductivity curve, water tends to remain steady and thus the fluctuation amplitude is smaller.

For the SBL with compaction degree of 0.93 (Figure 17(b)), the results at 15.4% and 30% fines content present the same reduction trend of $\Delta\theta$ from 4.6 m to 4.2 m. Then, the values stay stable from 4.2 m to 3.5 m for 15.4%. By contrast, the values of 5% are higher than the other two cases from 4.6 m to 3.5 m, while the curve overlapped with that of 15.4% at the elevation of 3.5 m. Compared to the effect of compaction degree, the fines content has a less impact on the fluctuation amplitude of volumetric water content.

## Conclusions

A numerical model of double-line high-speed railway track-bed was established to study the moisture migration in the substructure due to rainfall. Two fissures were set at the joint edges of the left-line concrete base and SSL, to simulate infiltrating boundaries in rainy days. A fitting relationship between rainfall duration time and daily precipitation was proposed. The effects of degree of compaction and fines content of SBL on the moisture migration in the substructure were investigated by numerical simulation, applying and analyzing the 2013 rainfall data of Hangzhou, China for a three-year period.

The results show that after a three-year period, the saturation zones exist in all cases. The size of saturation zone increases with degree of compaction or fines content, due to higher water retention capacity and lower hydraulic conductivity. And the fines content seems to present a greater impact.

The left-fissure profile is selected as the dangerous area to have a further analysis about volumetric water content variations in the subgrade. The arriving time of wetting front $t_{wf}$ and the fluctuation amplitude of volumetric water content $\Delta\theta$ after the arrival of wetting front are different for each case. It appears that both parameters are more influenced by degree of compaction than by fines content. A threshold value may exist between 0.90 and 0.93 degrees of

compaction, leading to a sudden increase of $t_{wf}$. For all cases, the time for the wetting front to pass through the interface of SSL and SBL is relatively long and drainage methods are needed to drain out the rainwater before infiltrating into the SBL.

## Declaration of Conflicting Interests

The author(s) declared no potential conflicts of interest with respect to the research, authorship, and/or publication of this article.

## Funding

## References

1. TB10621-2009. Code for design of high speed railway. The Ministry of Railways of the People's Republic of China, Beijing, China, 2009.
2. Aw ES. *Low cost monitoring system to diagnose problematic rail bed: case study at mud pumping site*. PhD Thesis, Massachusetts Institute of Technology, USA, 2007.
3. Berggren EG, Nissen A and Paulsson A. Track deflection and stiffness measurements from a track recording car. *Proc IMechE, Part F: J Rail and Rapid Transit* 2014; 228: 570–580.
4. Burrow MPN, Bowness D and Ghataora GS. A comparison of railway track foundation design methods. *Proc IMechE, Part F: J Rail and Rapid Transit* 2007; 221: 1–12.
5. Duong TV, Cui YJ, Tang AM, et al. Investigating the mud pumping and interlayer creation phenomena in railway sub-structure. *Eng Geol* 2014; 171: 45–58.
6. Li SW. The discussion of methods to deal with mud pumping in railway embankment. *Highw Eng* 2008; 33: 135–138.
7. Yang XA and Gao YL. GPR inspection for Shanghai Nanjing railway trackbed. *Chin J Rock Mech Eng* 2004; 23: 116–119.
8. Zhang WC, Su Q, Liu T, et al. Research on vibration characteristics of ballastless track subgrade under frost boiling at subgrade bed. *Rock Soil Mech* 2014; 35: 3556–3568.
9. Jiang HG, Bian XC, Jiang JQ, et al. Dynamic performance of high-speed railway formation with the rise of water table. *Eng Geol* 2016; 206: 18–32.
10. Alobaidi I and Hoare D. Factors affecting the pumping of fines at the subgrade subbase interface of highway pavements: a laboratory study. *Geosynthetics Int* 1994; 1: 221–259.
11. Bouazza A, Singh RM, Rowe RK, et al. Heat and moisture migration in a geomembrane-GCL composite liner subjected to high temperatures and low vertical stresses. *Geotext Geomembr* 2014; 42: 555–563.
12. Poulose A, Nair SR and Singh DN. Centrifuge modeling of moisture migration in silty soils. *J Geotech Geoenviron Eng* 2000; 126: 748–752.
13. Wang TH and Su LJ. Experimental study on moisture migration in unsaturated loess under effect of temperature. *J Cold Reg Eng* 2010; 24: 77–86.
14. Wang MW, Li J, Ge S, et al. Moisture migration tests on unsaturated expansive clays in Hefei, China. *Appl Clay Sci* 2013; 79: 30–35.
15. Gavin K and Xue JF. A simple method to analyze infiltration into unsaturated soil slopes. *Comput Geotechnics* 2008; 35: 223–230.
16. Tong YW, Luo R and Lytton RL. Modeling water vapor diffusion in pavement and its influence on fatigue crack growth of fine aggregate mixture. *Transport Res Rec* 2013; 2373: 71–80.
17. Zheng JL, Mai CQ and Zhang JH. A mathematical model for subgrade soil water-vapor migration. In: *2nd international conference on applied mechanics and materials (ICAMM 2013)*, Zhuhai, China, 23–24 November 2013.
18. Rahardjo H, Indrawan IGB, Leong EC, et al. Effects of coarse-grained material on hydraulic properties and shear strength of top soil. *Eng Geol* 2008; 101: 165–173.
19. ASTM D2487-11. Standard practice for classification of soils for engineering purposes (unified soil classification system). ASTM International, West Conshohocken, PA, 2011.
20. Duong TV, Trinh VN, Cui YJ, et al. Development of a large-scale infiltration column for studying the hydraulic conductivity of unsaturated fouled ballast. *Geotech Test J* 2013; 36: 1–10.
21. Chen RP, Wu J, Qi S, et al. A method for measuring hydraulic parameters of coarse-grained soils for high-speed railway subgrade. *Rock Soil Mech* 2015; 36: 3365–3372.
22. Wu J. *Experimental research on hydraulic characteristic of coarse-grained soils of high-speed railway subgrade*. Master Thesis, Zhejiang University, China, 2015.
23. van Genuchten MT. A closed-form equation for predicting the hydraulic conductivity of unsaturated soils. *Soil Sci Soc Am J* 1980; 44: 892–898.
24. Lu N and Kaya M. A drying cake method for measuring suction-stress characteristic curve, soil-water-retention curve, and hydraulic conductivity function. *Geotech Test J* 2013; 36: 1–19.
25. Zhang LM and Fredlund DG. Characteristics of water retention curves for unsaturated fractured rocks. In: *Second Asian conference on unsaturated soils,* Osaka, Japan, 10–12 November 2003.
26. Chae BG, Choi JH, Ichikawa Y, et al. Analysis of the permeability characteristics along rough-walled fractures using a homogenization method. *Nucl Eng Technol* 2012; 44: 43–52.
27. Wang HL, Chen RP, Luo L, et al. Numerical modeling of moisture migration in high-Speed railway subgrade. In: *International Symposium on Systematic Approaches to Environmental Sustainability in Transportation*, Fairbanks, Alaska, USA, 2–5 August 2015.
28. Webster GS. Discussion on maximum rates of rainfall at Boston. *Trans Am Soc Civil Eng* 1905; LIV: 204–210.
29. Zhou ZH, Wang H, Jia YW, et al. Temporal downscaling daily precipitation in lack-data watershed_ a case study in Yellow River. *Resour Sci* 2005; 27: 92–96.
30. McQueen IS and Miller RF. Approximating soil moisture characteristics from limited data: empirical

evidence and tentative model. *Water Resour Res* 1974; 10: 521–527.

31. Lu N and William JL. *Unsaturated soil mechanics*. Hoboken, NJ: John Wiley and Sons, Inc, 2004.

32. Zhang LM and Chen Q. Predicting bimodal soil-water characteristic curves. *J Geotech Geoenviron Eng* 2005; 131: 666–670.

33. Lloret A, Villar MV, Sanchez M, et al. Mechanical behaviour of heavily compacted bentonite under high suction changes. *Géotechnique* 2003; 53: 27–40.

34. Dingman SL. *Physical hydrology*. Upper Saddle River, NJ: Prentice Hall, 2002.

35. Parkin GW, Gardner WH, Auerswald K, et al. Wetting front. *Part of the series Encyclopedia of Earth Sciences Series,* 2016, pp.830–835.

36. Smethurst JA, Clarke D and Powrie W. Factors controlling the seasonal variation in soil water content and pore water pressures within a lightly vegetated clay slope. *Géotechnique* 2012; 62: 429–446.